IJE TRANSACTIONS A: Basics Vol. 30, No. 1, (January 2017) 109-119

International Journal of Engineering

Journal Homepage: www.ije.ir

Sliding Friction Contact Stiffness Model of Involute Arc Cylindrical Gear Based on Fractal Theory

W. Yang, H. Li*, M. Dengqiu, W. Yongqiao, C. Jian

School of Manufacturing Science and Engineering, Sichuan University, Chengdu, China

PAPER INFO

Paper history:
Received 07 September 2015
Received in revised form 09 November 2016
Accepted 28 December 2016

Keywords:
Fractal Theory
Contact Stiffness Model
Involute Arc Cylindrical Gear
Numerical Simulation

ABSTRACT

Gear's normal contact stiffness played an important role in the mechanical equipment. In this paper, the M-B fractal model is modified and the contact surface coefficient is put forward to set up the fractal model, considering the influence of friction, which could be used to calculate accurately the involute arc cylindrical gears' normal contact stiffness based on the fractal theory and Hertz theory. The contact surface coefficient is an exponential function of the load, radius of curvature and tooth line radius. The simulation results validate the reasonability of the contact surface coefficient and correctness of the fractal model. The contact surfaced coefficient increases with the increase of the load, radius of curvature and tooth line radius; the normal contact stiffness increases with the increase of material properties parameters, radius of the gear, load and fractal dimension (when fractal dimension is greater than 1.85, the normal contact stiffness decreases). Meanwhile, the normal contact stiffness increases with the decrease of roughness and decreases exponentially or linearly with the increase of friction coefficient. Research results are the foundation of the further analysis of arc gear contact problems.

***doi**: 10.5829/idosi.ije.2017.30.01a.14*

NOMENCLATURE

$z(x)$	Hight of asperity profile [m]	$F_e(A)$	Asperity load in the elastic state [N]
x	Position coordinate of profile [m]	p_p	Pressure on the asperity in the plastic state [N]
D	Fractal dimension	$F_p(A)$	Asperity load in the plastic state [N]
G	Parameter of roughness	p_{pe}	Pressure on the asperity in the elastic-plastic state [N]
γ	A constant and greater than one, γ^n is spatial frequency of the random profile	R_T	Tooth trace radius [m]
n_l	An ordinal number about the profile stucture of the lowest cutoff frequency	z_1, z_2	Number of teeth
l	Actual interface cross section width after deformation [m]	B	Gear width [m]
l'	Transverse width of asperity before deformation [m]	S	Theoretical contact area of deformation section[m^2]
A'	Asperity contact area [m^2]	$\sum S$	Sum of two contact bodies'(cylinder) surface area[m^2]
δ	Asperity deformation [m]	χ	Integrative curvature radius of arc gear [m]
P_{max}	Maximum contact pressure [N]	c	Coefficient
E	General elastic modulus[MPa]	L	Length of contact section [m]
E_1, E_2	Elastic modulus of body-1 and body-2[MPa]	d_1, d_2	Reference circle [m]
		F	Unit line load

*Corresponding Author's Email: *houli4@163.com* (H. Li)

Please cite this article as: W. Yang, H. Li, M. Dengqiu, W. Yongqiao, C. Jian, Sliding Friction Contact Stiffness Model of Involute Arc Cylindrical Gear Based on Fractal Theory, International Journal of Engineering (IJE), TRANSACTIONS A: Basics Vol. 30, No. 1, (January 2017) 109-119

P_m	Critical yield pressure of asperity [N]	k_n	Asperity normal stiffness of joint surface[N/m]
K_f	Correction factor of sliding friction	K_n	Normal stiffness of joint surface[N/m]
f	Friction factor	$n'(A)$	New distribution function
A	Real area [m^2]	E'	Elastic modulus in the elastic-plastic state
A_{pc}	Critical contact area in full plastic state[m^2]	K_n^*	Dimensionless expression of normal stiffness
A_{ec}	Critical contact area in elastic state[m^2]	A_{ec}^*	Dimensionless critical elastic deformation area
p_e	Pessure on the asperity in the elastic state [N]	A_a	Nominal contact area. [m^2]
$F_{pe}(A)$	Asperity load in the elastic-plastic state	p^*	Total dimensionless load [N]
$n(A)$	Distribution function of asperity	A_r^*	Dimensionless real contact area
A_l	Asperity maximum contact area [m^2]	A_{pc}^*	Dimensionless critical plastic deformation area
A_r	Real area of sliding friction surface [m^2]	F_z	Total load [N]
N	Quantity of asperities	d_1', d_2'	Pitch circle diameter [m]
$F_2(i)$	Bridging function, and i is integer ranging from 1 to 4	$F_1(i)$	Bridging function, and i is integer ranging from 1 to 4
G^*	Dimensionless parameter of roughness	A_l^*	Dimensionless asperity maximum contact area
Greek Symbols		ψ	Fractal region expansion coefficient;
ρ	Top curvature radius of asperity[m]	ν_1, ν_2	Poisson's ratio of body^{-1} and body^{-2}
δ	Asperity deformation [m]	ρ_g	Integrative curvature radius of arc gear [m]
σ_y	Softer material's yield strength [MPa]	α_t	Pressure angle of reference circle end face[^{o}]
δ_{ec}	Critical elastic deformation [m]	ρ_{n1} , ρ_{n2}	Normal curvature radius of node [m]
δ_{pc}	Full plastic deformation [m]	β_b	Tooth trace angle[^{o}]
ϕ	Material characteristic parameter	ε_a	Transverse contact ratio
λ	Impact factor of contact nodes	α_{a1}, α_{a2}	Addendum circle pressure angle[^{o}]
Subscripts		y	yield
1.2	Gear-1 and gear-2	*g*	Gear
e	Elastic	*p*	Plastic
ec	Critical elastic deformation	*pc*	Critical plastic deformation
pe	Plastic-elastic deformation state	*n*	Normal
t	Transverse contac	*r*	Real

1. INTRODUCTION

The buckling or chatter vibration might happen because of lack of stiffness in engineering, machinery, bridges, buildings, vehicles and ships. So enough structure stiffness is required in the design. A lot of works on the dynamic characteristics of machine have been done by many researchers for a long time [1-4]. The traditional ways of calculating the normal contact stiffness of involute arc cylindrical gear (called arc gear) were finite element analysis and Hertz theory, which used to make use of geometric parameters, material parameters and boundary conditions etc. However, consideration of microcosmic characteristics was inadequate. The fractal theory was a new scientific method, and a series of fractal models of contact stiffness and contact mechanics were developed, one of the most typical models was M-B fractal model [5]. Simulation analysis showed the influence of microcosmic parameters on fractal model. Wen Shuhua et al. [6] established the stiffness fractal model for fixed joint interfaces and gave a method to calculate fractal parameters. Wei Long et al. [7] established the sliding friction surface contact mechanics model and discussed the influence of different factors on A_r when f=0.1,ϕ=0.01. He also gave the relation between the pressure and contact area using a cubic polynomial in the elastic-plastic stage. Shuyun et al. [8] established a contact stiffness model of machined plane to study the contact between planes machined by different methods. However, all above models paid less attention to macro properties of contact surfaces, such as geometry of contact bodies and contact ways. The model was established mainly for the contact properties analyses of two planes, which was not suitable for cylinder surfaces' analyses. Hence, Zhao Han et al. [9] modified and expanded the fractal model and set up the normal stiffness model of two cylinder bodies. With the new model, he discussed the influence of different factors on tangential contact stiffness between cylinders' joint interface where $R_1 = 100mm, R_2 = 60mm$. However, he ignored the friction factor, which had nonlinear vibration properties. Therefore, Li Xiaopeng et al. [10, 11] set up the fractal model of cylinder bodies, which paid more attention to friction.In his paper, f ranged from 0 to 0.8. At present, the study about the arc gear is mostly based on the finite element analysis and Hertz theory [12-15]. Finite element analysis is based on the 3-D model. However, there is usually no 3-D model in the design, it is possible to lead to rework by choosing experientially parameters. On the other hand, as for Hertz theory, the gear strength design parameters couldn't be chosen from related graphic of straight gear and helical gear; but fractal model could solve related problems. Therefore, it is necessary to study joint surface of arc gear by fractal model.

In this paper, the fractal model of normal contact stiffness between two arc gears' joint surfaces is established by combination of macro and micro perspective based on the Hertz theory and fractal model, considering the influence of friction. The influence of relevant parameters on the normal contact stiffness is revealed with numerical simulation. Research results are the foundation of the further analysis of arc gear contact problems.

2. DISCUSSION OF ASPERITY DEFORMATION AND LOAD

2. 1. Discussion of Asperity Deformation

According to fractal theory, the mechanical surface with fractal characteristics could be described by W-M function [16]:

$$z(x) = G^{(D-1)} \sum_{n=n_l}^{\infty} \gamma^{-(2-D)n} \cos\left(2\pi\gamma^n x\right) \tag{1}$$

where $z(x)$ is hight of asperity profile, x is position coordinate of profile, D is fractal dimension, G is parameter of roughness, γ is a constant and greater than one, γ^n is spatial frequency of the random profile, n_l is an ordinal number about the profile stucture of the lowest cutoff frequency.

In Figure 1, ρ is the top curvature radius of asperity, l is actual interface cross section width after deformation, l' is transverse width of asperity before deformation. The relation between asperity contact area A' and l' is $l'=2\sqrt{A'/\pi}$. When $-l'/2 < x < l'/2$, the surface profile is cosine wave.

$$z(x) = G^{D-1} l'^{2-D} \cos\frac{\pi x}{l'} \left(-l'/2 < x < l'/2\right) \tag{2}$$

According to Equation (2), the top curvature radius of asperity ρ is:

$$\rho = \left| \frac{\left[1+(z')^2\right]^{3/2}}{|z''|} \right|_{x=0} = \frac{l'^D}{\pi^2 G^{D-1}} = \frac{2^D A'^{D/2}}{\pi^{(4+D)/2} G^{D-1}} \tag{3}$$

Combining Figure 1 and Equation (2), the asperity deformation δ is:

$$\delta = z(0) = G^{D-1} l'^{2-D} = 2^{2-D} G^{D-1} \left(\frac{A'}{\pi}\right)^{(2-D)/2} \tag{4}$$

1) The critical elastic deformation of asperity. According to Hertz theory, when asperity deformation is in elastic state, the maximum contact pressure $P_{\max}$ is [16]:

$$P_{\max} = \frac{2E}{\pi}\left(\frac{\delta}{\rho}\right)^{\frac{1}{2}} \tag{5}$$

where, E is the general elastic modulus, and $E = \left(\frac{1-\nu_1^2}{E_1} + \frac{1-\nu_2^2}{E_2}\right)^{-1}$, E_1, E_2 are elastic modulus of body-1 and body-2; ν_1, ν_2 are Poisson's ratio of body-1 and body-2.

Considering the relative sliding friction existing in contact bodies, the critical yield pressure of asperity P_m is [17]:

$$P_m = 1.1 K_f \sigma_y \tag{6}$$

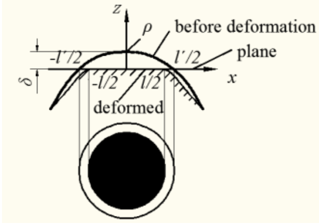

Figure 1. Asperity deformation

where, σ_y is softer material's yield strength; K_f is the correction factor of sliding friction [18], and $K_f = \begin{cases} 1\text{-}0.228f & 0 \le f \le 0.3 \\ 0.932\exp\left[-1.58\left(f-0.3\right)\right] & 0.3 < f \le 0.9 \end{cases}$, f is friction factor.

According to reference [17], the relation between real area A and A' is $A = A'/2$ when asperity deformation is in the elastic state. According to Equation (3, 5-6), when the maximum contact pressure $P_{\max}$ is equal to the critical yield pressure of asperity P_m, the asperity critical elastic deformation δ_{ec} could be obtained, represented as

$$\delta_{ec} = \frac{2^{3D/2} A^{D/2}}{\pi^{D/2} G^{D-1}} \left(\frac{11 K_f \phi}{20} \right)^2 \tag{7}$$

where, ϕ is material characteristic parameter, and $\phi = \sigma_y / E$.

When the asperity is in the elastic stage, combining Equation (4) and the relationship $A = A'/2$, the relation between asperity deformation δ and real area A is:

$$\delta = \frac{2^{3(2\text{-}D)/2}}{\pi^{(2\text{-}D)/2}} G^{D-1} A^{(2\text{-}D)/2} \tag{8}$$

If $\delta_{ec} = \delta$, combining Equation (7) and Equation (8), critical contact area in elastic state A_{ec} is:

$$A_{ec} = \frac{\pi}{8} G^2 \left(\frac{20}{11 K_f \phi} \right)^{2/(D-1)} \tag{9}$$

2) The critical plastic deformation of asperity. Deformation style changes with curvature radius. In order to make sure the accuracy of the contact stress analysis, it is necessary to distinguish plastic and elastic-plastic deformation. Assuming δ_{pc} is the full plastic deformation, when the asperity deformation δ is larger than δ_{pc}, asperity is in the elastic-plastic deformation state. Now, $A' = A$ [17].

According to Johnson theory [17], asperity is in the full plastic deformation state when $El'/\left(\sigma_y \rho\right) \approx 60$. $El'/\left(\sigma_y \rho\right) \approx 60$ is a condition to distinguish the plastic deformation and the elastic-plastic deformation. In this paper, combining Equation (3) and Johnson theory, the expression of A' is Equation (10) at critical plastic deformation point.

$$A' = \left(\frac{\pi^{\frac{4+D}{2}} G^{D-1} El'}{60 \times 2^D \sigma_y} \right)^{\frac{2}{D}} \tag{10}$$

And $l' = 2\sqrt{A'/\pi}$, $A' = A$. According to Equation (10), the critical contact area in full plastic state A_{pc} is:

$$A_{pc} = G^2 \left(\frac{\pi^{3+D}}{900 \phi^2 4^D} \right)^{1/(1-D)} \tag{11}$$

In conclusion, if $A < A_{pc}$, asperity deformation is in the full plastic deformation state; $A_{pc} < A < A_{ec}$, asperity deformation is in the elastic-plastic deformation state; $A > A_{ec}$, asperity deformation is in the elastic deformation state.

2. 2. Relation Between Asperity Load and Contact Area

1) The relation between load and contact area when asperity is in the elastic state. The pressure on the asperity p_e [16] is:

$$p_e = \frac{4E}{3\pi} \left(\frac{\delta}{\rho} \right)^{\frac{1}{2}} \tag{12}$$

And the asperity load $F_e(A)$ is:

$$F_e(A) = p_e A = \frac{2^{(7-3D)/2} \pi^{(D-1)/2}}{3} E G^{D-1} A^{(3-D)/2} \tag{13}$$

2) The relation between load and contact area when asperity is in the plastic state. Considering the influence of sliding friction, plastic deformation asperity contact pressure p_p [19] is:

$$p_p = 1.1 K_f \sigma_y \tag{14}$$

And the asperity load $F_p(A)$ is:

$$F_p(A) = p_p A = 1.1 K_f \sigma_y A \tag{15}$$

3) The relation between load and contact area when asperity is in the elastic-plastic state. When elastic and plastic deformation exist at the same time, the relation between contact area and contact loading becomes quite complex. However, the pressure of two critical deformation points couldn't mutate, namely the changing of critical points' contact pressure and deformation should be continuous. According to reference [20], when asperity is in the elastic-plastic state, the relation between load and contact area could be expressed as a polynomial function, where elastic-plastic deformation of the contact area ranges from A_{pc} to A_{ec}. The elastic-plastic deformation asperity contact pressure's p_{pe} boundary condition is defined as:

When $A = A_{pc} \Rightarrow p_{pe} = p_p, dp_{pe}/d_A = dp_p/d_A$

When $A = A_{ec} \Rightarrow p_{pe} = p_e, dp_{pe}/d_A = dp_e/d_A$

According to Hermite interpolation method, the expression for p_{pe} in terms of A is a cubic polynomial function. Taking a sample function for a cubic polynomial, $y=3x^2 - 2x^3$. The function increases monotonously in the interval [0, 1], and the boundary values are $x=0, y=0$ and $x=1, y=1$.

Assuming $x=\frac{A-A_{pc}}{A_{ec}-A_{pc}}$, $A=A_{pc}$ and $A=A_{ec}$ are respectively corresponding with $x=0$ and $x=1$.

According to the cubic polynomial, the elastic-plastic deformation contact pressure p_{pe} is**:**

$$p_{pe}=p_{pc}-\left(p_{pc}-p_{ec}\right)\left[3\left(\frac{A-A_{pc}}{A_{ec}-A_{pc}}\right)^2-2\left(\frac{A-A_{pc}}{A_{ec}-A_{pc}}\right)^3\right] \tag{16}$$

$$\begin{aligned} F_{pe}(A)=p_{pe}A=1.1K_f\sigma_f A-(1.1K_f\sigma_f \\ -\frac{2^{(7-3D)/2}\pi^{(D-1)/2}}{3}EG^{D-1}A_{ec}^{(1-D)/2})\times \\ \left[3\left(\frac{A-A_{pc}}{A_{ec}-A_{pc}}\right)^2-2\left(\frac{A-A_{pc}}{A_{ec}-A_{pc}}\right)^3\right]A \end{aligned} \tag{17}$$

3. FRACTAL MODEL OF INVOLUTE ARC CYLINDRICAL GEAR

According to fractal theory, distribution function of asperity $n(A)$ was represented as [7]:

$$\begin{cases} n(A)=\frac{D}{2}\psi^{(2-D)/2}A_l^{D/2}A^{-(D+2)/2} \\ \frac{\psi^{(2-D)/2}-\left(1+\psi^{-D/2}\right)^{-(2-D)/D}}{(2-D)/D}=1 \\ A_l=\frac{2-D}{D}\psi^{(D-2)/2}A_r \end{cases} \tag{18}$$

where, ψ is fractal region expansion coefficient; A is asperity contact area; A_l is asperity maximum contact area; A_r is real area of sliding friction surface.

This distribution function applies to two planes. Obviously, when the contact faces were curved surface, quantity of asperities N would change. In theory, quantity of asperities increase with the increase of contact area, but N is always less than $n(A)$. Therefore, the form of contact faces has influence on quantity of asperities.

3. 1. Modification of Distribution Function

Arc gear is a new kind of gear, and its model which is modeled by UG software is showed in Figure 2. The following two are its main characteristics: tooth trace is part of the arc; tooth profile curve is involute spur.

1) According to reference [15], touch strength of gear is always calculated at gear node. The integrative curvature radius of arc gear ρ_g is

$$\rho_g=\frac{\rho_{n1}\rho_{n2}}{\rho_{n1}+\rho_{n2}}=\frac{d_1'd_2'\sin\alpha_t}{2\left(d_1'+d_2'\right)\cos\beta_b} \tag{19}$$

where, α_t is pressure angle of reference circle end face; ρ_{n1}, ρ_{n2} are the normal curvature radius of node, $\rho_{n1}=\frac{d_1'\sin\alpha_{t1}}{2\cos\beta_b}$, $\rho_{n2}=\frac{d_2'\sin\alpha_{t2}}{2\cos\beta_b}$; d_1', d_2' are pitch circle diameter; β_b is tooth trace angle.

2) Arc gear could be divided into width-infinitesimal gear along the direction of gear width. The total length of contact line is the sum of the contact line of divided gears, so the total length of contact line L is

$$L=\frac{2R_T\varepsilon_a}{\cos 20^\circ}\arcsin\frac{B\cos 20^\circ}{2R_T} \tag{20}$$

where, R_T is tooth trace radius; ε_a is transverse contact ratio, $\varepsilon_a=\frac{1}{2\pi}\left[z_1\left(\tan\alpha_{a1}-\tan\alpha_t\right)+z_2\left(\tan\alpha_{a2}-\tan\alpha_t\right)\right]$, z_1, z_2 are number of teeth, α_{a1}, α_{a2} are addendum circle pressure angle; B is gear width.

3) Assuming that two contact bodies are uniform in texture and isotropic, the quantities of asperities on the contact faces satisfy the following relation

$$n'(A)=\lambda n(A) \tag{21}$$

where, λ is impact factor of contact nodes, called contact surface coefficient.

Because the quantities of asperities on contact faces satisfy exponential function, assuming that contact surface coefficient is an exponential function, λ was represented as:

$$\lambda=\left(\frac{s}{\sum S}\right)^{\frac{x}{R_T{}^c}} \tag{22}$$

where, s is theoretical contact area of deformation

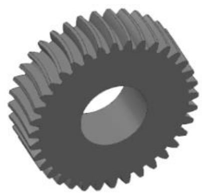

Figure 2. Involute arc cylindrical gear

section; $\sum S$ is the sum of two contact bodies'(cylinder) surface area; x is integrative curvature radius of arc gear, $x=\rho_g$; c is coefficient, $c=1/2$.

According to the Hertz theory, geometrical shape of deformed section is rectangle. S is the product of deformed width of contact section $4\left(\frac{F\rho_g}{\pi E}\right)^{\frac{1}{2}}$ and the length of contact section L (length of contact line), represented as:

$$s=4L\left(\frac{F\rho_g}{\pi E}\right)^{\frac{1}{2}} \tag{23}$$

where, F is unit line load.

The contact of the gear could be regarded as the contact of the two deformed cylinders showed in Figure 3. The radius of two cylinders is respectively the normal curvature radius of node ρ_{n1}, ρ_{n2}. Therefore, the contact area $\sum S$ represented as:

$$\sum S=2\pi\left(\rho_{n1}+\rho_{n2}\right)L \tag{24}$$

According to the Equations (19)-(20) and Equations (22)-(24), Equation (22) can be rewritten as:

$$\lambda=\left[\frac{\left(\frac{8F}{\pi E}\frac{d_1d_2\sin\alpha_t\cos\beta_b}{\left(d_1+d_2\right)}\right)^{\frac{1}{2}}}{\pi\left(d_1+d_2\right)\sin\alpha_t}\right]^{\frac{2\left(d_1+d_2\right)\cos\beta_b}{d_1d_2\sqrt{R_T}\sin\alpha_t}} \tag{25}$$

where, d_1, d_2 are reference circle, and $d_1=d_1'$, $d_2=d_2'$ (standard installation) Assuming that F=1000 N, B=35 mm, R_T=50 mm, $E=2\times10^{11}$ Pa, d_1=125 mm and d_2 could be changed; Figure 4 (a) could be obtained.

It revealed that λ was always less than 1. It meant that λ satisfied assumption, quantities of asperities on contact faces were always less than $n(A)$. When d_2 approached 0, λ approached 0; d_2 was approached infinite, λ approached 1,but it was always less than 1, now, which was equivalent to contact between cylindrical surface and plane, but it was still different from M-B model, so λ must be theoretically less than 1.

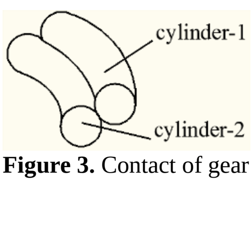

Figure 3. Contact of gear

Changing F, and ensuring other conditions to be fixed, Figure 4 (b) could be obtained. When F approached 0, λ was minimum, not equal to 0, there was no contact stress, but there was contact, so λ wasn't equal to 0. With the increase of F, λ increased within a narrow range, and was always less than 1. Because the asperity always existed on contact faces, complete contact was impossible. The changing trend of λ with R_T was showed in the Figure 4 (c), λ increased with the increase of R_T, R_T was tending to be infinite, λ was always less than 1, it agreed to limit of λ. In conclusion, the choice about λ is reasonable.

Based on the reasonable analysis of λ, the new distribution function was put forward in this paper, represented as:

$$\begin{aligned} n'(A) &= \lambda\frac{D}{2}\psi^{\frac{(2-D)}{2}}A_l^{\frac{D}{2}}A^{-\frac{(D+2)}{2}} \\ &= \frac{D}{2}\psi^{\frac{(2-D)}{2}}A_l^{\frac{D}{2}}\times \\ & A^{-\frac{(D+2)}{2}}\left[\frac{\left(\frac{8F}{\pi E}\frac{d_1d_2\sin\alpha_t\cos\beta_b}{(d_1+d_2)}\right)^{\frac{1}{2}}}{(d_1+d_2)\sin\alpha_t}\right]^{\frac{2(d_1+d_2)\cos\beta_b}{d_1d_2\sqrt{R_T}\sin\alpha_t}} \end{aligned} \tag{26}$$

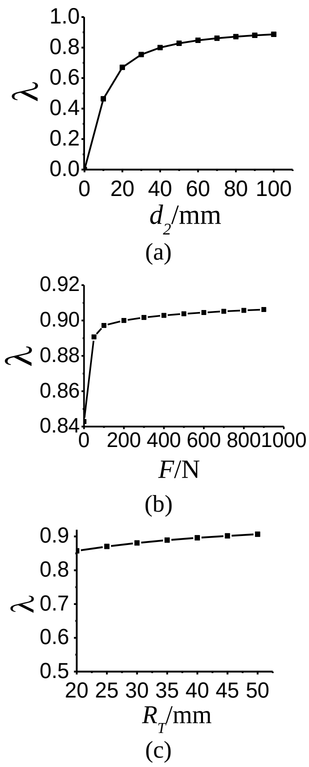

Figure 4. (a) Changing trend of λ with d_2 (b) Changing trend of λ with F (c) Changing trend of λ with R_T

3. 2. Arc Gear Normal Contact Stiffness According to reference [21], the asperity normal stiffness of joint surface k_n is

$$k_n = 2E\left(A/\pi\right)^{\frac{1}{2}} \tag{27}$$

The normal stiffness of joint surface K_n is

$$K_n = \int k_n n'(A)dA \tag{28}$$

The asperity deformation has elastic stage, elastic-plastic stage and plastic stage. However, each asperity deformation is just one of three deformations. The normal stiffness represents the ability of resisting plastic deformation. According to reference [10], in the elastic-plastic stage, stress decreases, deformation increases, and elastic modulus decreases, so elastic modulus $E' = 0.9E$. There exists no stiffness in the plastic stage. So, the normal stiffness of joint surface K_n can be rewritten as**:**

$$\begin{aligned} K_n &= \int_{A_{ec}}^{A_l} k_n n'(A)dA + \int_{A_{pc}}^{A_{ec}} k_n n'(A)dA = \\ &\frac{2\lambda DE'}{\sqrt{\pi}(1-D)}\left(\frac{2-D}{D}\right)^{D/2} \psi^{(D-2)^2/4} A_r^{\ D/2}(A_{ec}^{(1-D)/2} \\ &- A_{pc}^{(1-D)/2}) + \frac{2\lambda DE}{\sqrt{\pi}(1-D)}\left(\frac{2-D}{D}\right)^{D/2} \psi^{(D-2)^2/4} \times \\ &A_r^{\ D/2}\left(\left(\frac{2-D}{D\psi^{(2-D)/2}}\right)^{(1-D)/2} A_r^{\ (1-D)/2} - A_{ec}^{(1-D)/2}\right) \end{aligned} \tag{29}$$

Equation. (29) can be rewritten as dimensionless expression K_n^*

$$\begin{aligned} K_n^* &= \frac{2\lambda D}{\sqrt{\pi}(1-D)}\left(\frac{2-D}{D}\right)^{D/2} \psi^{(D-2)^2/4} A_r^{*D/2} \times \\ &\left(\left(\frac{2-D}{D\psi^{(2-D)/2}}\right)^{(1-D)/2} A_r^{*(1-D)/2} - A_{ec}^{*(1-D)/2}\right) \\ &+ \frac{1.8\lambda D}{\sqrt{\pi}(1-D)}\left(\frac{2-D}{D}\right)^{D/2} \psi^{(D-2)^2/4} A_r^{*D/2} \times \\ &\left(A_{ec}^{*\,(1-D)/2} - A_{pc}^{*(1-D)/2}\right) \end{aligned} \tag{30}$$

where, A_r^* is dimensionless real contact area, $A_r^* = A_r/A_a$; A_{ec}^* is dimensionless critical elastic deformation area, $A_{ec}^* = A_{ec}/A_a$; A_{pc}^* is dimensionless critical plastic deformation area, $A_{pc}^* = A_{pc}/A_a$; A_a is nominal contact area.

According to the relation among real area, critical elastic deformation area and critical plastic deformation area, the relation between real area and asperity load could be divided into following three situations.

when $A_l \le A_{pc}$, total load $F_z = \int_0^{A_l} F_p(A)n(A)dA$, divided both sides by $A_a E$. The total dimensionless load expression of p^* is:

$$p^* = 1.1\lambda K_f \phi A_r^* \tag{31}$$

when $A_{pc} < A_l < A_{ec}$, total load $F_z = \int_0^{A_{pc}} F_p(A) \times n(A)dA + \int_{A_{pc}}^{A_l} F_{pe}(A)n(A)dA$, divided both sides by $A_a E$. Total dimensionless load expression of p^* is:

$$\begin{aligned} p^* &= 1.1\lambda K_f \phi A_r^* + \lambda K(D) g_1(D) A_r^{*\frac{D}{2}} \times \\ &\quad (H_1(D) - H_2(D)) \\ H_1(D) &= \frac{3}{(A_{ec}^* - A_{pc}^*)^3}[F_1(3) - 2F_1(2)A_{pc}^* \\ &\quad + F_1(1)A_{pc}^{*\,2}] \\ H_2(D) &= \frac{2}{(A_{ec}^* - A_{pc}^*)^3}[F_1(4) - \\ &\quad 3F_1(3)A_{pc}^* + 3F_1(2)A_{pc}^{*\,2} - F_1(1)A_{pc}^{*\,3}] \\ K(D) &= 1.1K_f\phi - \frac{2^{(7-3D)/2}\pi^{(D-1)/2}}{3} \times \\ &\quad G^{*D-1}A_{ec}^{*(1-D)/2} \end{aligned} \tag{32}$$

where, $g_1(D) = \frac{D}{2}\left(\frac{2-D}{D}\right)^{D/2} \psi^{(2-D)^2/4}$; $F_1(i)$ is bridging function, and i is integer ranging from 1 to 4, $F_1(i) = \frac{2}{2i-D}\left(A_l^{*(2n-D)/2} - A_{pc}^{*(2n-D)/2}\right)$; $G^* = G/\sqrt{A_a}$; $A_l^* = \frac{A_l}{A_a} = \frac{(2-D)A_r^*}{D\psi^{(2-D)/2}}$. When $A_l \ge A_{ec}$, the total load $F_z = \int_0^{A_{pc}} F_p(A) \times n(A)dA + \int_{A_{pc}}^{A_{ec}} F_{pe}(A)n(A)dA + \int_{A_{ec}}^{A_l} F_e(A) \times n(A)dA$, divided both sides by $A_a E$. The total dimensionless load expression of p^* is:

When $D \ne 1.5$

$$\begin{aligned} p^* &= \lambda G^{*D-1} g_2(D) A_r^{*\frac{D}{2}}\left[g_3(D) A_r^{*\frac{3-2D}{2}} - A_{ec}^{*\frac{3-2D}{2}}\right] \\ &\quad + 1.1\lambda K_f \phi g_4(D) A_r^{*\frac{D}{2}} A_{ec}^{*\frac{2-D}{2}} \\ &\quad + \lambda K(D) g_1(D) A_r^{*\frac{D}{2}} \times \left(H_3(D) - H_4(D)\right) \\ H_3(D) &= \frac{3}{(A_{ec}^* - A_{pc}^*)^2} \times [F_2(3) - 2F_2(2)A_{pc}^* \\ &\quad + F_2(1)A_{pc}^{*\,2}] \\ H_4(D) &= \frac{2}{(A_{ec}^* - A_{pc}^*)^3} \times [F_2(4) - 3F_2(3)A_{pc}^* \\ &\quad + 3F_2(2)A_{pc}^{*\,2} - F_2(1)A_{pc}^{*\,3}] \\ K(D) &= 1.1\lambda K_f\phi - \frac{2^{(7-3D)/2}\pi^{(D-1)/2}}{3} \times \\ &\quad G^{*D-1}A_{ec}^{*(1-D)/2} \end{aligned} \tag{33}$$

When $D = 1.5$

$$p^* = \frac{\pi^{\frac{1}{4}}}{6^{\frac{3}{4}}} \lambda \psi^{\frac{1}{16}} G^{*\frac{1}{2}} A_r^{*\frac{3}{4}} \ln \frac{A_l^*}{A_{ec}^*} + 1.1 \times 3^{\frac{1}{4}} \lambda K_f \phi \psi^{\frac{1}{16}} A_r^{*\frac{3}{4}} A_{ec}^{*\frac{1}{4}} - \frac{3^{\frac{1}{4}}}{4} \lambda \psi^{\frac{1}{16}} A_r^{*\frac{3}{4}} K(D) \times \left(H_3(D) - H_4(D) \right) \tag{34}$$

where $g_2(D) = \frac{2^{(7-3D)/2} \pi^{(D-1)/2} D}{3(3-2D)} \left(\frac{2-D}{D} \right)^{D/2} \psi^{(2-D)^2/4}$;

$g_3(D) = \left(\frac{2-D}{D \psi^{(2-D)/2}} \right)^{(3-2D)/2}$; $g_4(D) = \left(\frac{D}{2-D} \right)^{(2-D)/2} \psi^{(2-D)^2/4}$;

$F_2(i) = \frac{2}{2i-D} \left(A_{ec}^{*(2n-D)/2} - A_{pc}^{*(2n-D)/2} \right)$, and i is integer ranging from 1 to 4.

4. PARAMETERS ANALYSES OF ARC GEAR FRACTAL MODEL

4. 1. The Influence of Load on the Normal Contact Stiffness

The influence of load on the normal contact stiffness was revealed in Figure 5. Simulation showed that normal contact stiffness increased with the increase of contact load, and the bigger D was, the faster the increase rate was. Because of the contact area A_r increased with the contact load, which would lead to the increase of resistance capacity to deformation. Therefore, it was beneficial to improve the normal stiffness by increasing the contact load.

4. 2. The Influence of Fractal Dimension on the Normal Contact Stiffness

The influence of fractal dimension on the normal contact stiffness was revealed in Figure 6.

Simulation showed that normal contact stiffness increased nonlinearly with the increase of fractal dimension, because the critical deformation area decreased with the increase of fractal dimension, resulting in the increase of quantities of elastic deformation asperity, stiffness was improved.

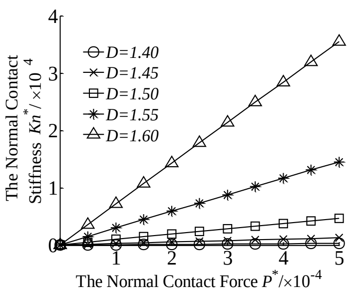

Figure 5. Relation curves between stiffness and contact force at different fractal dimensions

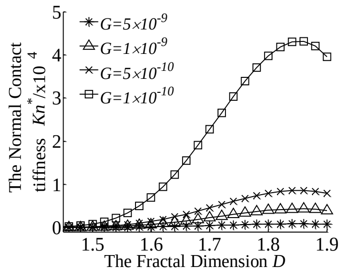

Figure 6. Relation curves between stiffness and fractal dimension at different characteristic length scales

However, when D was greater than 1.85, normal contact stiffness decreased with the increase of fractal dimension, because the outline became more and more refined with the increase of fractal dimension, and quantities of plastic and elastic-plastic deformation asperity added. Finally, the stiffness decreases. What's more, the smaller parameter of roughness was, the bigger rate of increase or decrease was. Therefore, it was beneficial to improve the normal stiffness by increasing reasonably the fractal dimension.

4. 3. The Influence of Parameter of Roughness on Stiffness

The influence of parameter of roughness on stiffness was revealed in Figure 7. Simulation showed that normal contact stiffness increased with the decrease of roughness on stiffness, rate of increase was bigger with bigger load and smaller parameter of roughness. Therefore, it was beneficial to improve the normal stiffness by decreasing parameter of roughness.

4. 4. The influence of Friction Coefficient on Stiffness

The influence of friction coefficient on stiffness was revealed in Figure 8.

Simulation showed that normal contact stiffness decreased with the increase of friction coefficient. When the friction coefficient was between 0 and 0.3, the normal contact stiffness decreased linearly with the increase of friction coefficient; when the friction coefficient was between 0.3 and 1, the normal contact stiffness decreased exponentially with the increase of friction coefficient.

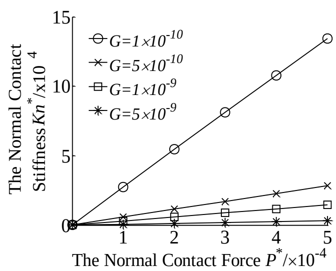

Figure 7. Relation curves between stiffness and contact force at different roughness

Rate of decrease became smaller with the increase of fractal dimension. Therefore, it was beneficial to improve the normal stiffness by decreasing friction coefficient at bigger fractal dimension.

4. 5. The Influence of Material Properties Parameters on Stiffness The influence of material properties parameters on stiffness was revealed in Figure 9. Simulation showed that normal contact stiffness increased with the increase of material properties parameters. $\phi = \sigma_y / E$, σ_y is softer material's yield strength. Therefore, it was beneficial to improve the normal stiffness by improving softer material's yield strength.

4. 6. The Influence of Contact Surface Coefficient on Stiffness The influence of contact surface coefficient on stiffness was revealed in Figure 10. Figure 10 (b) is the magnifying figure.

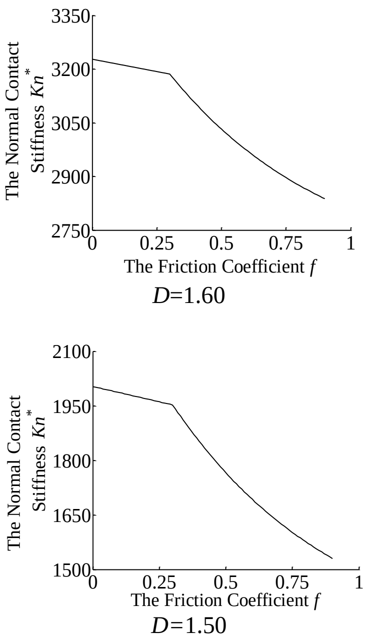

Figure 8. Relation curves between stiffness and friction coefficient at different fractal dimensions

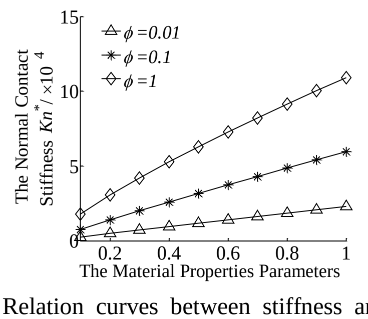

Figure 9. Relation curves between stiffness and material properties parameters at different fractal dimensions

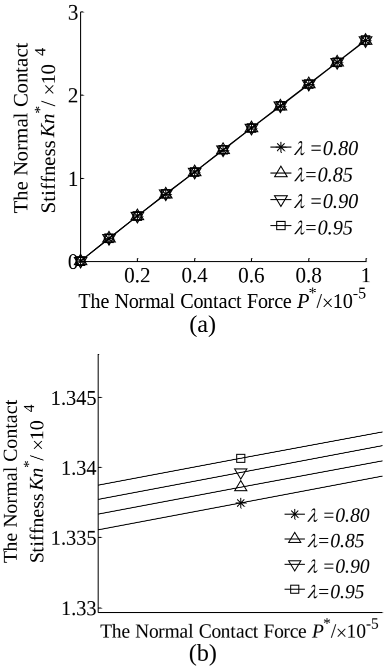

Figure 10. Relation curves between stiffness and contact force at different contact surface coefficient

Simulation showed that normal contact stiffness increased with the increase of contact surface coefficient at the same load, but rate of decrease wasn't big. According to Figure 4, the contact surface coefficient increased with the increase of gear radius and load. Therefore, it was beneficial to improve the normal stiffness by increasing gear radius and load.

5. CONCLUSION

In this paper, the M-B fractal model was modified and the contact surface coefficient was put forward to set up the fractal model, considering the influence of friction, which could be used to calculate accurately normal contact stiffness between two arc gears' joint interfaces based on the fractal theory and Hertz theory. The simulation results validated the reasonability of the contact surface coefficient and revealed the contact surfaced coefficient increased with the increase of the load, radius of curvature and tooth line radius.

Simulation results showed that the normal contact stiffness increased nonlinearly with the increase of fractal dimension. However, when fractal dimension was greater than 1.85, the normal contact stiffness decreased with the increase of fractal dimension. In addition, the smaller parameter of roughness caused the bigger rate of increase or decrease and the normal contact stiffness increased with the decrease of roughness and increase of material properties parameters, radius of the gear and load. Furthermore, when the friction coefficient was between 0 and 0.3, the stiffness decreased linearly with the increase of friction coefficient. When the friction coefficient was between 0.3 and 1, the stiffness decreased exponentially with the increase of friction coefficient, and rate of decrease became smaller with the increase of fractal dimension.

Many parameters of model were selected empirically in the simulation. It must be careful to calculate the stiffness of actual product by the fractal model of normal contact stiffness, although simulation showed that the model was right in theory. In order to settle the problem, the authors will do test and validate study for the normal contact stiffness in following study.

6. ACKNOWLEDGE

This project is supported by National Natural Science Foundation of China (Grant No. 51375320).

7. REFERENCES

1. Korrani, M.A. and Mahani, M.F., "Dynamic analysis of a three-rotor flexible coupling with angular misalignment", ***International Journal of Engineering-Transactions B: Applications***, Vol. 24, No. 2, (2011), 155-164.
2. Jahanmiri, M. and Abbaspour, M., "Experimental investigation of drag reduction on ahmed model using a combination of active flow control methods", ***International Journal of Engineering-Transactions A: Basics***, Vol. 24, No. 4, (2011), 403-410.
3. Toloei, A., Aghamirbaha, E. and Zarchi, M., "Mathematical model and vibration analysis of aircraft with active landing gear system using linear quadratic regulator technique", ***International Journal of Engineering-Transactions B: Applications***, Vol. 29, No. 2, (2016), 137-144.
4. Shooshtari, A. and Razavi, S., "Nonlinear vibration analysis of rectangular magneto-electro-elastic thin plates", ***International Journal of Engineering-Transactions A: Basics***, Vol. 28, No. 1, (2014), 136-147.
5. Majumdar, A. and Bhushan, B., "Fractal model of elastic-plastic contact between rough surfaces", ***Journal of Tribology***, Vol. 113, No. 1, (1991), 1-11.
6. Shuhua, W., Zongyang, Z. and Xueliang, Z., "Stiffness fractal model for fixed joint interfaces", ***Transactions of the Chinese Society for Agricultural Machinery***, Vol. 44, No. 2, (2013), 255-260.
7. Wei, L., Liu, Q. and Zhang, P., "Sliding friction surface contact mechanics model based on fractal theory", ***Jixie Gongcheng Xuebao(Chinese Journal of Mechanical Engineering)***, Vol. 48, No. 17, (2012), 106-113.
8. Jiang, S., Zheng, Y. and Zhu, H., "A contact stiffness model of machined plane joint based on fractal theory", ***Journal of Tribology***, Vol. 132, No. 1, (2010), 011401.
9. Chen, Q., Huang, K., Zhao, H. and Zhang, Y., "Simulation and analysis of the model of calculating contact tangential stiffness between cylinders' joint interfaces by matlab", in Applied Mechanics and Materials, Trans Tech Publ. Vol. 190, (2012), 177-181.
10. Li, X., Guo, H., Liu, J., Nie, H. and Wen, B., "Fractal model and simulation of normal contact stiffness considering the friction between joint surfaces", ***Journal of Vibration, Measurement & Diagnosis***, Vol. 33, No. 2, (2013), 210-213.
11. Li, X., Zhao, G., Liang, Y. and Ju, X., "Fractal prediction model and simulation of contact stiffness considering friction factors between joint surfaces", ***International Journal of Industrial and Systems Engineering***, Vol. 18, No. 3, (2014), 418-431.
12. Tseng, J.-T. and Tsay, C.-B., "Mathematical model and surface deviation of cylindrical gears with curvilinear shaped teeth cut by a hob cutter", ***Journal of Mechanical Design***, Vol. 127, No. 5, (2005), 982-987.
13. Lia, B.W., Y. Li, H. and You, H., "Modelling and numerical simulation of cutting stress in end milling of titanium alloy using carbide coated tool", ***International Journal of Engineering Transactions A Basic***, Vol. 28, No. 7, (2015), 1900-1908.
14. Wang, S.-J., Hou, L., Dong, L. and Xiao, H.-J., "Modeling and strength analysis of cylindrical gears with curvilinear shape teeth for manufacture", ***Journal of Sichuan University: Engineering Science Edition***, Vol. 44, No. 2, (2012), 210-215.
15. WANG, Z.-l., SONG, A.-p., CHEN, T. and WANG, S.-f., "Contact stress analysis of the involute arc cylindrical gear pair", ***Machinery Design & Manufacture***, Vol. 12, (2008), 188-191.
16. Bhushan, B., "Introduction to tribology, John Wiley & Sons, (2013).
17. Johnson, K.L. and Johnson, K.L., "Contact mechanics, Cambridge university press, (1987).
18. Wang, S. and Komvopoulos, K., "A fractal theory of the interfacial temperature distribution in the slow sliding regime: Part-multiple domains, elastic-plastic contacts and applications", ***Journal of Tribology***, Vol. 116, No. 4, (1994), 824-832.
19. Guoan, C. and Shirong, G., "Prediction model of sliding wear during running-in process based on fractal theory", ***Chinese Journal of Mechanical Engineering***, Vol. 36, No. 2, (2000), 29-33.
20. Yongwu, Z., Yanming, L. and Jianzhong, J., "New elastic-plastic model for the contact of rough surfaces", ***Chinese Journal of Mechanical Engineering***, Vol. 43, No. 3, (2007), 95-101.
21. Zhang, X., Huang, Y., Fu, W. and Zhang, W., "Fractal model of normal contact stiffness between rough surfaces", ***Chin. J. Appl. Mech***, Vol. 17, No. 2, (2000), 31-35.

Sliding Friction Contact Stiffness Model of Involute Arc Cylindrical Gear Based on Fractal Theory

W. Yang, H. Li, M. Dengqiu, W. Yongqiao, C. Jian

School of Manufacturing Science and Engineering, Sichuan University, Chengdu, China

PAPER INFO

Paper history:
Received 07 September 2015
Received in revised form 09 November 2016
Accepted 28 December 2016

Keywords:
Fractal Theory
Contact Stiffness Model
Involute Arc Cylindrical Gear
Numerical Simulation

چکیده

سفتی تماس عادی دنده نقش مهمی در تجهیزات مکانیکی ایفا کرده است. در این مقاله، مدل فراکتال MB اصلاح شد و ضریب سطح تماس برای راه اندازی مدل فراکتال، با درنظرگرفتن تاثیر اصطکاک ها که می تواند برای محاسبه دقیق سفتی تماس عادی قوس گستران استوانه ای بر اساس تئوری فراکتال و نظریه هرتز مورد استفاده قرار گیرد، رو به جلو به قرار داده شده است. ضریب سطح تماس، تابع نمایی از بار، شعاع انحنا و دندان شعاع خط است. نتایج شبیه سازی، منطقی بودن ضریب سطح تماس و درستی مدل فراکتال را اعتبار می بخشد. ضریب سطح تماس با افزایش بار، شعاع انحنا و خط دندان شعاع افزایش می یابد، سختی تماس عادی با افزایش خواص پارامترهای مواد، شعاع چرخ دنده، بار و بعد فرکتال افزایش می یابد (هنگامی که بعد فرکتال بیشتر از ۱/۸۵ است، سختی تماس عادی کاهش می یابد). در همین حال، سفتی تماس عادی با کاهش زبری افزایش و به صورت نمایی و یا خطی با افزایش ضریب اصطکاک کاهش می یابد. نتایج تحقیقات پایه و اساس تجزیه و تحلیل بیشتر از مشکلات تماس دنده قوس است.

***doi**: 10.5829/idosi.ije.2017.30.01a.14*